Food and Chemical Toxicology 154 (2021) 112352

Contents lists available at ScienceDirect

Food and Chemical Toxicology

journal homepage: www.elsevier.com/locate/foodchemtox

Dietary nanoparticles alter the composition and function of the gut microbiota in mice at dose levels relevant for human exposure

Laeticia Perez [a,1], Eleonora Scarcello [a,1], Saloua Ibouraadaten [a], Yousof Yakoub [a], Riccardo Leinardi [a], Jérôme Ambroise [b], Bertrand Bearzatto [b], Jean-Luc Gala [b], Adrien Paquot [c], Giulio G. Muccioli [c], Caroline Bouzin [d], Sybille van den Brule [a], Dominique Lison [a,*]

[a] Université catholique de Louvain, Institut de Recherche Expérimentale et Clinique, Louvain centre for Toxicology and Applied Pharmacology, Avenue Hippocrate 57, 1200, Brussels, Belgium
[b] Université catholique de Louvain, Institut de Recherche Expérimentale et Clinique, Centre de Technologies Moléculaires Appliquées, Clos Chapelle-aux-champs 30, 1200, Brussels, Belgium
[c] Université catholique de Louvain, Louvain Drug Research Institute, Bioanalysis and Pharmacology of Bioactive Lipids Research Group, Avenue Mounier 73, B1.72.01, 1200, Brussels, Belgium
[d] IREC Imaging Platform (2IP), Institut de Recherche Expérimentale et Clinique, UCLouvain, Brussels, Belgium

ARTICLE INFO

Handling editor: Dr. Jose Luis Domingo

Keywords:
Ag NP
SiO_2 NP
TiO_2 NP
Food
Lipid metabolism
Long-term effects

ABSTRACT

Background: Nanotechnologies provide new opportunities for improving the safety, quality, shelf life, flavor and appearance of foods. The most common nanoparticles (NPs) in human diet are silver metal, mainly present in food packaging and appliances, and silicon and titanium dioxides used as additives. The rapid development and commercialization of consumer products containing these engineered NPs is, however, not well supported by appropriate toxicological studies and risk assessment. Local and systemic toxicity and/or disruption of the gut microbiota (GM) have already been observed after oral administration of NPs in experimental animals, but results are not consistent and doses used were often much higher than the estimated human intakes. In view of the strong evidence linking alterations of the GM to cardiometabolic (CM) diseases, we hypothesized that dietary NPs might disturb this GM-CM axis.

Materials and methods: We exposed male C57BL/6JRj mice (n = 13 per dose group) to dietary NPs mixed in food pellets at doses relevant for human exposure: Ag (0, 4, 40 or 400 μg/kg pellet), SiO_2 (0, 0.8, 8 and 80 mg/kg pellet) or TiO_2 (0, 0.4, 4 or 40 mg/kg pellet). After 24 weeks of exposure, we assessed effects on the GM and CM health (n = 8 per dose group). The reversibility of the effects was examined after 8 additional weeks without NPs exposure (recovery period, n ≤ 5 per dose group).

Results: No overt toxicity was recorded. The GM β-diversity was dose-dependently disrupted by the three NPs, and the bacterial short chain fatty acids (SCFAs) were dose-dependently reduced after the administration of SiO_2 and TiO_2 NPs. These effects disappeared completely or partly after the recovery period, strengthening the association with dietary NPs. We did not observe atheromatous disease or glucose intolerance after NP exposure. Instead, dose-dependent decreases in the expression of IL-6 in the liver, circulating triglycerides (TG) and urea nitrogen (BUN) were recorded after administration of the NPs.

Conclusion: We found that long-term oral exposure to dietary NPs at doses relevant for estimated human intakes disrupts the GM composition and function. These modifications did not appear associated with atheromatous or deleterious metabolic outcomes.

1. Introduction

Because of their unique mechanical, physicochemical and biological properties, engineered nanomaterials are increasingly used worldwide in many fields, including the food industry (Chaudhry et al., 2008; Fruijtier-Polloth, 2016). Among these nanomaterials, silver (Ag), silicon dioxide (SiO_2) and titanium dioxide (TiO_2) nanoparticles (NPs) are the

* Corresponding author.
E-mail addresses: laeticia.perez@uclouvain.be (L. Perez), dominique.lison@uclouvain.be (D. Lison).
[1] both authors contributed equally.

https://doi.org/10.1016/j.fct.2021.112352
Received 27 April 2021; Received in revised form 2 June 2021; Accepted 12 June 2021
Available online 18 June 2021
0278-6915/© 2021 The Authors. Published by Elsevier Ltd. This is an open access article under the CC BY-NC-ND license (http://creativecommons.org/licenses/by-nc-nd/4.0/).

Abbreviation

ALAT	alanine aminotransferase
ASV	amplicon sequence variants
bw	body weight
B6	C57BL/6JRj
BUN	blood urea nitrogen
CM	cardiometabolic
GM	gut microbiota
GTT	glucose tolerance test
HDL	high density lipoproteins
HDL-c	HDL-cholesterol
H&E	hematoxylin and eosin
HTS	high-throughput sequencing
IL	interleukin
LCN	lipocalin
NOEL	no observed effect level
NP	nanoparticle
PBS	phosphate-buffered saline
PCoA	principal coordinates analysis
PVP	polyvinylpyrrolidone
SAA	serum amyloid A
SCFA	short chain fatty acid
SD	standard deviation
TG	triglycerides

most commonly used in food products (McClements and Xiao, 2017). Ag NPs are added in confectionery as decorative covering (E174) or in food packaging for their antibacterial properties (Hajipour et al., 2012). SiO_2 NPs (E551) are incorporated as anticaking agents to some powdered foods, such as salt, spices or dried milk, to enhance flow properties (Dekkers et al., 2011). TiO_2 NPs (E171), which contains up to 43% of NPs (Dorier et al., 2017), are used as whitening agents in candies, chewing gums or bakery (Fiordaliso et al., 2018). The human dietary intake of these NPs is estimated at 1 μg Ag/kg bw/day (van den Brule et al., 2016), 2 mg SiO_2/kg bw/day (Dekkers et al., 2011) and 1 mg TiO_2/kg bw/day (Weir et al., 2012).

The consumption of these NPs, added directly to food or migrated from packaging, has long been considered toxicologically harmless (Fruijtier-Polloth, 2016). However, some studies have suggested that food NPs are able to induce local and/or systemic toxicity, raising concerns about possible health risks (Pietroiusti et al., 2017). Weight loss, epithelial cell damage in intestinal microvilli, severe inflammation of the colon, as well as oxidative hepatic toxicity, inflammation or lipid metabolism dysregulation have been observed in rats or mice orally exposed to high doses of Ag NPs (up to 2.5 mg/kg bw/d) (Chen et al., 2017; Orr et al., 2019; Ebabe Elle et al., 2013). Regarding SiO_2 NPs, long-term studies in rats or mice have reported contrasting results. Liver and kidney toxicity has been recorded after chronic oral administration of SiO_2 NPs (Chen et al., 2017; Meike van der Zande et al., 2014; So et al., 2008), whereas other studies did not record toxicity (Kim et al., 2014; Yoshida et al., 2014; Murugadoss et al., 2017). In mice, intestinal inflammation and preneoplastic lesions of the colon have been observed after short-term oral exposure to 10 mg TiO_2 NPs/kg bw/d (Bettini et al., 2017; Mu et al., 2019). In rats, subchronic exposure to the same dose of TiO_2 NPs induced liver and cardiovascular toxicity as well as decreased plasma triglycerides levels (Chen et al., 2015, 2019a; Jensen et al., 2018a). A recent evaluation of E171 by the European Food Safety Agency (EFSA) concluded that "Based on all the evidence available, a concern for genotoxicity could not be ruled out, and given the many uncertainties, the Panel concluded that E171 can no longer be considered as safe when used as a food additive" (Younes et al., 2021).

The potential impact of food NPs on the GM has also been investigated, but the conclusions remain elusive, and doses used were often higher than the currently estimated human intakes. Gut dysbiosis has been recorded by some of us after the ingestion of Ag NPs at human relevant doses (11.4 μg/kg bw/d) in a 28-day study in mice (van den Brule et al., 2016), and by William et al. (Williams et al., 2015) in a longer study (13 weeks) with a higher dose range in rats (up to 36 mg/kg bw/d). However, the GM alterations reported in both studies differed as Williams et al. (2015) documented a decrease in the Firmicutes/Bacteroidetes ratio, whereas we (van den Brule et al., 2016) reported an increase of the same ratio. In contrast, rats (Hadrup et al., 2012) and mice (Wilding et al., 2016) exposed during 28 days to 9 and 10 mg Ag NPs/kg bw/d, respectively, did not show alterations of the GM composition. A single short-term exposure (7 days) study in mice, using SiO_2 NPs (2.5 mg/kg bw/d) documented an increase in gut microbial richness and diversity (Chen et al., 2017). Regarding TiO_2 NPs, a short-term exposure study (7 days) in mice exposed to 10 mg/kg bw/d did not report alterations of the GM (Chen et al., 2019b), whereas exposure to the same dose during 3 months reduced the abundance of several probiotic taxa, including *Bifidobacterium* and *Lactobacillus* (Mu et al., 2019). Longer exposure (28 days) to a very high dose of TiO_2 NPs (100 mg/kg bw/d) did not affect the GM diversity but shifted its structure, with Proteobacteria being significantly increased by rutile but not by anatase NPs (Li et al., 2018).

The GM is often considered as a forgotten or hidden organ, interacting with the human body (O'Hara and Shanahan, 2006). Increasing evidence has demonstrated that the GM participates in physiological functions of the host, and several studies have indicated that alterations of the GM can be associated with adverse health effects, including cardiometabolic (CM) diseases such as atheromatosis, diabetes, obesity, or lipid disorders (Pascale et al., 2018). In view of this close relationship, a CM toxicity of dietary NPs, mediated by GM dysbiosis, appears plausible. This concern is supported by the well-documented cardiovascular toxicity of ambient ultrafine particles (Robertson and Miller, 2018; Rajagopalan et al., 2018), which can also affect the GM after respiratory clearance and swallowing (Li et al., 2017a; Mutlu et al., 2018; Wang et al., 2018).

Here, we designed a long-term exposure study in mice (24 weeks), at doses relevant for the estimated human intakes, to investigate the possible impact of the three main food NPs (Ag, SiO_2 and TiO_2) on the GM-CM axis. To better document the causal relationship between the observed effects and NPs ingestion, the reversibility of the effects was assessed after a recovery period of 8 weeks during which mice were fed standard pellets. The mouse was selected as experimental model as this species is extensively used in toxicological studies, especially for cardiovascular and metabolic disorders (Russell and Proctor, 2006; Kennedy et al., 2010). It is also a good model for GM studies as C57Bl/6 mice in particular share bacterial communities with humans, similar at the phylum level (Hugenholtz and de Vos, 2018). Male mice were used to avoid the hormonal confounding of estrogens that influence cardiovascular functions (Morselli et al., 2017).

2. Materials & methods

2.1. Nanoparticles

Polyvinylpyrrolidone (PVP)-coated Ag NPs were obtained from Sigma-Aldrich (purity 99.5%, 576832-5G, Vial # MKBN3581V, St Louis, MO) and have been extensively characterized in a previous study (van den Brule et al., 2016). JRCNM2002a and JRCNM10200a (similar to NM100) were obtained from the JRC repository (European Commission – DG JRC, Ispra, Italy) as representatives of dietary SiO_2 and TiO_2 NPs,

respectively. An extensive physicochemical characterization of these reference samples is available in Rasmussen et al. (2013) and Rasmussen et al. (2014), respectively. The main physicochemical characteristics of the NPs are summarized in Table 1.

2.2. Preparation of food supplemented with NPs

As the objective of the study was to use dose ranges relevant for human dietary exposure, we selected, for each NP, a dose range which integrates the estimated human daily intake. Assuming an average mouse body weight of 20 g and a daily food consumption of 5 g per mouse, we calculated the concentrations of NP needed in food to reach the respective intake doses. The NPs were incorporated to the food pellets by the producer, starting from powdered Altromin standard diet 1324 (Carfil, Oud-Turnhout, Belgium). Food bags were stored at room temperature, in dark and dry conditions. New batches of Ag NPs were prepared every month to avoid sulfidation by food components (van den Brule et al., 2016). NPs intake doses and corresponding concentrations in food are reported in Table 2.

2.3. Animal and experimental design

Four-week-old male C57BL/6JRj mice (B6 mice) were purchased from Janvier Labs (St Bertevin, France). Upon arrival, the mice were quarantined in the local facility (Animalerie Centrale, UCLouvain, Brussels, Belgium) in positive-pressure air-conditioned units (25 °C, 50% relative humidity, 16:8 h light/dark cycle, sterile rodent food and acidified water *ad libitum*). After 2 weeks of acclimation, we homogenized the GM by mixing the cage litters twice a week during two weeks before initiation of NP exposure. Then, a total of 156 eight-week-old mice were identified by individual ear tags and randomly assigned to 12 experimental groups of 13 mice each (Fig. 1). For each experimental group, the 13 mice were distributed in 3 different cages (5, 4 and 4 mice per cage). Animals were then fed for 24 weeks with NP-supplemented food. Mice were weighed weekly during exposure, and food consumption was recorded weekly per cage. One mouse in the 0 μg Ag/kg food group died during the glucose tolerance test (see 2.4) and three mice (one in the 0 μg Ag/kg food group, one in the 4 μg Ag/kg food group, and one in the 40 mg food TiO_2/kg group) died during an intestinal permeability test, not reported in this manuscript. After 24 weeks of exposure, 8 mice randomly drawn from the 3 cages of each dose group were euthanized by an intra-peritoneal injection of pentobarbital. Intracardiac blood was collected and plasma was isolated after centrifugation for 15 min at 4 °C and 240 *g*. The right medial lobe of the liver was resected and snap frozen at −80 °C. Cecal contents were collected and stored at −20 °C. The distal portion of the ileum and the proximal colon were excised (3 cm each), rinsed with NaCl 0.9%, and preserved in 4% formaldehyde at 4 °C. Finally, the thoracic aorta was dissected, opened longitudinally, and fixed in 4% formaldehyde. The remaining mice per dose group (n = 3–5) were fed control pellets (Altromin standard diet) for eight additional weeks (recovery period) and then sacrificed as above. We did not exclude any animal from the analyses. The experimental plan is outlined on Fig. 1.

Table 1
Main physicochemical properties of the test nanoparticles.

	AgNPs	SiO_2 NPs	TiO_2 NPs
Type	Metallic	Pyrogenic	Anatase
Average primary size (nm)	<100	15.5	110
Specific surface area (m^2/g)	5	204	9
Other elements (% weight)	PVA[a]	Al (0.45), Ca (0.18)	Fe (0.28), Si (0.09), Al (0.49)
Food quality	Yes	Yes	Yes

[a] PVP = polyvinylpyrrolidone.

Table 2
NP intake doses and concentrations in food.

	NP intake doses	NP concentrations in food
Ag NPs	0, 1, 10 or 100 μg/kg bw/d	0, 4, 40 or 400 μg/kg pellet
SiO_2 NPs	0, 0.2, 2 or 20 mg/kg bw/d	0, 0.8, 8 or 80 mg/kg pellet
TiO_2 NPs	0, 0.1, 1 or 10 mg/kg bw/d	0, 0.4, 4 or 40 mg/kg pellet

2.4. Glucose tolerance test (GTT)

After 20 weeks of exposure, we randomly selected 5 mice per dose group for an oral glucose tolerance test. Mice were fasted 6 h before the administration of a glucose load (2 g/kg bw in a volume of 150 μl water) by oral gavage (Bowe et al., 2014). Glucose was measured with a glucometer (Accu Check® AVIVA, Roche, Switzerland) in blood from the tail vein, before glucose administration and at regular intervals thereafter (after 15, 30, 60 and 120 min). After the GTT, mice were returned to their cages and further fed food supplemented in NPs.

2.5. Analysis of inflammatory biomarkers

2.5.1. Systemic inflammation

Systemic inflammation was assessed by measuring serum amyloid (SA) A-1 and interleukin (IL)−6 mRNA expression in the liver by RT-qPCR. Livers were homogenized with an Ultra-Turrax® (IKA) in 2 ml of TriPure, and total RNA extraction was performed according to the manufacturer's protocol (Roche, Mannheim, Germany). RNA concentration was measured by absorbance at 260 nm (SpectraMax® iD3). First-strand cDNA synthesis was performed with 2 μg of RNA, oligo-(dT) primers (Eurogentech, Seraing, Belgium) and M-MLV RT (Invitrogen, Carlsbad, CA). Quantitative PCR was performed on 10-fold diluted samples in sterile UltraPure® water (Invitrogen). PCR master mix (SYBR Green, Applied Biosystems, Foster City, CA) and primers (300 nM) were added to samples (5 μl) and 20 μl were loaded in 96-well PCR plate to perform the PCR (StepOnePlus Real-Time PCR System, Applied Biosystems, Foster City, CA). Sequences of interest were amplified using the following forward primers 5′-CAGGAGACACCAGGATGAAGC-3' (SAA-1); 5′-GAGGATACCACTCCCAACAGACC-3' (IL-6); 5′-CGGCTACCACATCCAAGGAA-3' (18S rRNA) and reverse primers 5′-GGAAAGCCTCGTGAACAAATG-3' (SAA-1); 5′-CACAACTCTTTTCTCATTTCCACG-3' (IL-6); 5′-ATACGCTATTGGAGCTGGAATTACC-3' (18S rRNA). The PCR program was as follows: 10 min 95 °C, (15 sec 95°C, 1 min 60 °C) x40. After amplification, a melting curve was generated to check that the amplified double-stranded DNA products belonged to a single discrete species of the correct size (verified by agarose gel electrophoresis), and data analysis was performed with the StepOne™ Software v2.3 (Applied Biosystems). Results were calculated as ratio of SAA-1 or IL-6 expression to the expression of the 18S rRNA gene.

2.5.2. Intestinal inflammation

Intestinal inflammation was evaluated by measuring lipocalin (LCN)-2 concentration in cecal content and in serum using an enzyme-linked immunosorbent assay (ELISA). Frozen cecal samples (50 mg) were diluted in 0.5 ml of phosphate buffer saline (PBS) containing 0.1% Tween 20, vortexed for 20 min to get a homogenous suspension, and then centrifuged for 10 min at/15,000 *g* (4 °C). Analysis was performed on clear supernatants using the Duoset murine LCN-2 ELISA kit (R&D Systems, Minneapolis, MN). Serum samples were diluted 1000 times in BSA 1% in PBS before analysis.

2.6. Clinical chemistry

Triglycerides (TG), total cholesterol, high-density lipoprotein -cholesterol (HDL-C), alanine aminotransferase (ALAT), and blood urea nitrogen (BUN) were measured in plasma samples with an automated

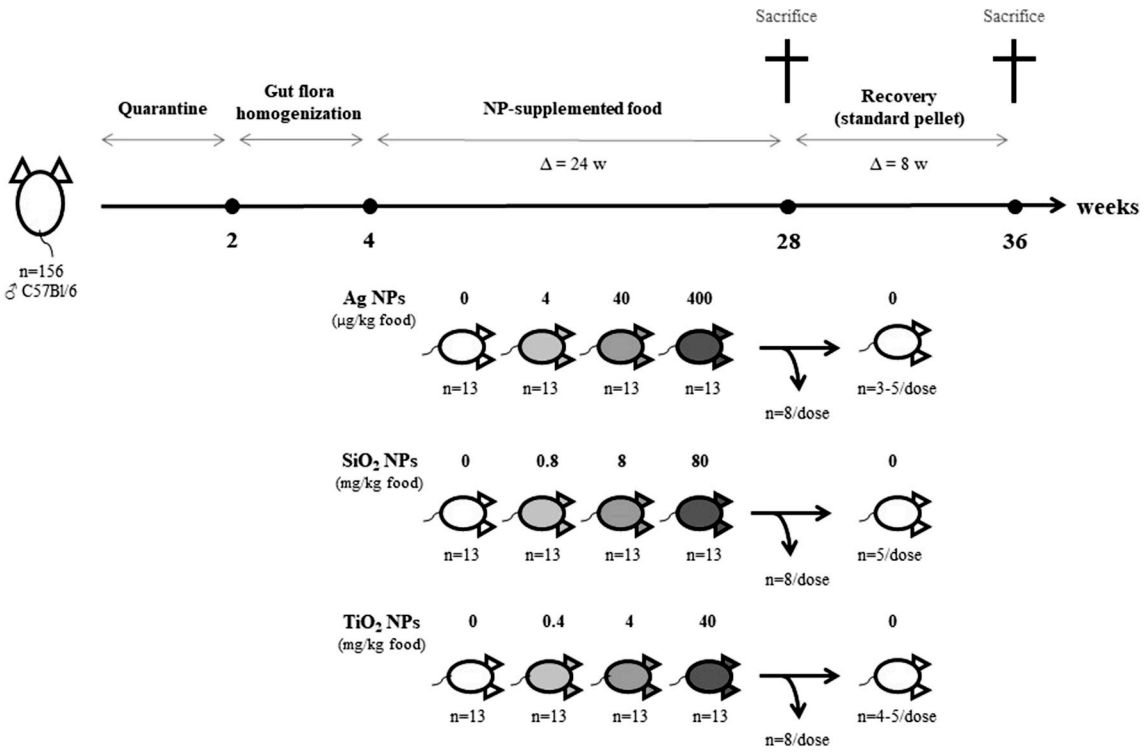


Fig. 1. Experimental design. Male B6 mice were fed normal diet during the quarantine (2 weeks) and the GM homogenization periods (2 additional weeks). Animals were then randomly assigned to the different groups fed NP-supplemented diet (Ag, SiO_2 or TiO_2) at different doses for 24 weeks. After 28 weeks, 96 (8 x 4 x 3) mice were sacrificed to evaluate the CM effects and the impact on GM. The 5 remaining mice per dose were fed a normal diet for 8 additional weeks to evaluate the reversibility of the effects (recovery period). n = number of animals.

dry chemistry analyzer (Fuji Dri-chem Nx500, Fujifilm Co., Tokyo, Japan).

2.7. Lipid staining of thoracic aorta

Each preserved aorta was rinsed for 5 min in PBS, incubated for 5 min in 60% 2-propanol, stained for 45 min in Oil Red O (0.5% stock solution diluted 3:2 in distilled water) at 37 °C under continuous agitation, washed again for 5 min in 60% 2-propanol and finally repeatedly rinsed with distilled water. Aortas were inspected *en face* with a binocular (16X magnification) and images were recorded.

2.8. Tissue staining for histopathologic analysis

The ileum and colon were embedded in paraffin. Tissues were sectioned with a microtome at 5-μm thickness and stained with hematoxylin & eosin (H&E) using standard protocols.

2.9. Short chain fatty acids analysis

Short chain fatty acids (SCFA) standards were purchased from Sigma Aldrich with the exception of acetic acid which was purchased from VWR Belgium. Valproic acid (internal standard), 3-nitrophenylhydrazine (3-NPH), N-(3-Dimethylaminopropyl)-N′-ethylcarbodiimide (EDC) and pyridine were purchased from Sigma Aldrich. HPLC and MS grade solvent (acetonitrile (ACN), chloroform and methanol) were purchased from VWR Belgium. For SCFA quantification, a derivatization method was used prior ultraperformance liquid chromatography coupled to mass spectrometry (UPLC-MS) analysis. Briefly, cecal contents (50–60 mg wet material) were homogenized in water (20 mg/50 μL) and then sonicated 10 min in an ice bath (4 °C). Fifty μl were transferred into tubes containing 200 μL ACN for protein precipitation and valproic acid as internal standard. After 1 h at −20 °C, samples were centrifuged and supernatants were transferred into glass tubes for derivatization (1 h, 40 °C) using 3-NPH in the presence of EDC and pyridine. Samples were then purified by liquid-liquid extraction using chloroform to remove the remaining reagents. The final residue was analyzed using an UPLC-LTQ Orbitrap XL instrument (ThermoFischer Scientific). A Hypersil GOLD PFP (100 × 2.1 mm; 1.9 μM) column maintained at 40 °C was used to achieve the SCFA separation. H_2O-ACN-acetic acid (94.9:5:0.1; v/v/v) and ACN-acetic acid (99.9:0.1; v/v) were used as mobile phase in gradient mode to separate the different isomers. For compound ionization, an APCI source operated in positive ionization mode was used. Xcalibur® software was used for data analysis. Ratio between the compound of interest and the internal standard was used for data normalization, and calibration curves processed using the same protocol were performed for each metabolite quantification. SCFA levels were then normalized to cecal content weight.

2.10. DNA extraction and 16S rRNA gene sequencing

DNA was extracted from cecal contents with a QIAamp Fast DNA Stool Mini kit according to manufacturer's guidelines (Qiagen, Hilden, Germany), except for DNA elution with molecular biology grade water (HyClone™, Waltham, Massachusetts). DNA extracts were quantified using a Qubit fluorometer (Invitrogen, Gent, Belgium) with a Qubit dsDNA HS Assay kit (DNA concentration varied between 5 and 25 ng/μl). AMPure XP beads (Beckman Coulter, Indianapolis, IN) were used to remove contaminants from the 16S DNA. Samples were then diluted using HyClone™ water in equal concentrations (5 ng/μl) and stored at −20 °C until high-throughput sequencing (HTS). Sequencing libraries were prepared according to the Illumina 16S metagenomic sequencing library preparation protocol (San Diego, CA) at the Center of Applied Molecular Technologies (CTMA, UCLouvain, Brussels, Belgium). In brief, the V3-V4 variable region of the 16S bacterial rRNA gene was amplified using a two-stage PCR protocol (Klindworth et al., 2013). The

first-stage PCR (PCR1) amplification uses universal primers of the interest region with overhang adapters attached (forward primer: 5′TCG TCG GCA GCG TCA GAT GTG TAT AAG AGA CAG CCT ACG GGN GGC WGC AG and reverse primer: 5′ GTC TCG TGG GCT CGG AGA TGT GTA TAA GAG ACA GGA CTA CHV GGG TAT CTA ATCC) to amplify a 483-bp portion of the V3-V4 region. This step uses a kit 2x KAPA HiFi HotStart ReadyMix in a mixture total volume of 25 μl per sample. The PCR1 was run under the following conditions: 3 min denaturation at 95 °C; 25 cycles of denaturation (30 s at 95 °C), annealing (30 s at 55 °C) and extension (30 s at 72 °C); a final extension at 72 °C for 5 min. The PCR1 product was cleaned with AMPure XP beads in a 0.8X ratio (Beckman Coulter, Indianapolis, IN) to purify the 16S V3-V4 amplicon from free primers and primer dimer species. The second-stage PCR (PCR2) was done with 5 μl PCR1 purified to attach dual indices and Illumina sequencing adapters using the Nextera XT v2 Index Kit D. The PCR2 was performed under the same conditions as PCR1 with only eight PCR cycles of denaturation/annealing/extension. A clean-up of the PCR2 products with AMPure XP beads (Beckman Coulter, Indianapolis, IN) was performed before quantification on a Qubit fluorometer (Invitrogen, Gent, Belgium). All libraries sizes were then evaluated by capillary electrophoresis on an Agilent Technologies 2100 Bioanalyzer using an Agilent DNA 1000 kit (Agilent Technologies). After quantification and size determination, all libraries were equimolarly pooled to a final concentration of 4 nM. After NaOH denaturation and dilution, a 9 pM pooled library was loaded on MiSeq reagent kits v3 (600 cycles) including Illumina 15% PhiX control spike-in.

Blanks consisting of sterile water instead of genetic material were performed to validate each laboratory step and to identify possible contamination (extraction, amplification and sequencing).

The metagenomics datasets generated and analyzed during the current study are available in the European Nucleotide Archive repository under study PRJEB44239 and PRJEB44281.

2.11. Sequencing data analysis

All NGS reads were processed using R 3.6.3 and the dada2 Bioconductor package (Callahan et al., 2016). Sequences were trimmed and filtered in order to tolerate a maximum of 2 expected errors per paired ends read. Amplicon sequence variants (ASV) were inferred using the high-resolution DADA2 method, which distinguishes sequencing errors from real biological variation. Chimeras and low abundance ASV making up <0.005% of reads were subsequently removed from the data set (Bokulich et al., 2013). Taxonomy was assigned with a naive Bayesian classifier implemented in the DADA2 package and using the Greengenes v13.8 training set. Sequencing data were rarefied to randomly select 30.000 paired-end reads per sample, using the phyloseq Bioconductor package. Data from blank samples were analyzed to control for potential contamination in DNA extraction kits, as previously recommended (Hornung et al., 2019).

The α-diversity indexes (i.e., richness, Simpson, Shannon) within the different microbial communities were calculated using the phyloseq Bioconductor package. In order to avoid potential biases due to a cage effect (Laukens et al., 2016) and considering that multiple cages (n = 3) housed the mice submitted to each NP dose, α-diversity indexes were assessed through mixed effects models with cage introduced as a random effect and the NP dose as a continuous, fixed effect.

To investigate differences in community composition (β-diversity), weighted UniFrac distances were calculated and plotted using principal coordinates analysis (PCoA) with the GUniFrac R package. The effects of NP dose on β-diversity were assessed through a permutational multivariate analysis of variance (PERMANOVA), using the Adonis function of the vegan package in R. As mixed effects models are not implemented in this package, the β-diversity analysis was performed on per cage average bacterial profiles.

To identify the bacterial genus, families and phyla that were impacted by each NP, ASV were grouped at the genus, family, and phylum level. The counts were then normalized to their relative abundance before applying centered log-ratio (CLR) transformation for compositional data, as previously described (Kong et al., 2020). Mixed effect models were built on the transformed data with cage introduced as a random effect and NP dose as continuous, fixed effect.

When the effect of NP dose was assessed on multiple outcomes (e.g. relative abundance of several families), p-values were corrected (Q-values) using the Benjamini-Hochberg methodology to control the false discovery rate (FDR) at 10% (Hochberg, 1995).

2.12. Statistical analyses

Except for sequencing data, graphs and statistical analyses were computed with GraphPad Prism 8.3 (GraphPad Software, La Jolla, CA). All results are presented as means ± standard deviation (S.D.) of n replicates. Differences between control and treated groups were assessed by analysis of variance (ANOVA) followed by a post-hoc Dunnett's multiple comparison and/or a linear trend test as appropriate. Differences with p-value < 0.05 or Q-+value < 0.1 were considered statistically significant.

3. Results and discussion

3.1. No overt systemic or digestive toxicity was recorded after NP exposure

Food consumption and body weight gain were not modified during the exposure period (24 weeks) (Figs. S1A–C) and after 8 weeks of recovery (Figs. S2A–C). Histological analyses did not reveal alterations of the intestinal epithelium integrity or villi structure after 24 weeks of exposure to the highest dose of each NP (Figs. S3A–B). The cecal and serum concentration of LCN-2, a sensitive biomarker of intestinal inflammation (Chassaing et al., 2012), did not reveal an impact of exposure (Figs. S4A–B).

Plasma ALAT activity, a marker of liver damage, was slightly but significantly increased after 24 weeks of SiO_2 NP administration (Fig. 2A), not after recovery (Fig. 2A'). No significant effect of Ag or TiO_2 NPs on plasma ALAT activity was recorded. The concentration of blood urea nitrogen (BUN) in plasma, a marker of renal function, was not increased but, instead, dose-dependently reduced after 24 weeks of NP exposure (Fig. 2B) and less after the recovery period (Fig. 2B'). The biological significance of this reduction of BUN plasma levels remains unclear. Urea is physiologically produced in the liver to detoxify ammonia, mainly produced by Gram negative bacteria in the gut (Hill and Drasar, 1975). Since we did not detect severe liver damage in the present study, a reduced production of ammonia by the GM (Collins and D'Orazio, 1993) appears as a plausible hypothesis to explain lowered circulating urea levels. We did, however, not detect specific GM composition changes which might account for a reduced ammonia production (see 3.2).

Overall, these results indicated that exposure to the three NPs, at dose levels relevant for human exposure, did not induce overt systemic or intestinal toxicity.

3.2. Dietary NP exposure altered the composition of the gut microbiota

Bacterial DNA was analyzed by HTS in cecal contents after 24 weeks of exposure to the NPs, and after 8 weeks of recovery. Alpha- and β-diversities, as well as the differential abundance of phyla, families and genera were analyzed. The linear mixed effect models built on α-diversity indexes (i.e., richness, Shannon, Simpson) for every NP did not reveal significant effects (Q-values > 0.10) neither after exposure (Fig. 3A–C) or after recovery (Fig. 3A'-C'). This is consistent with other studies in which mice were exposed to high doses of Ag NPs (10 mg/kg bw/d) or TiO_2 NPs (100 mg/kg bw/d) (Wilding et al., 2016; Li et al., 2018), but does not reproduce the decrease in bacterial evenness

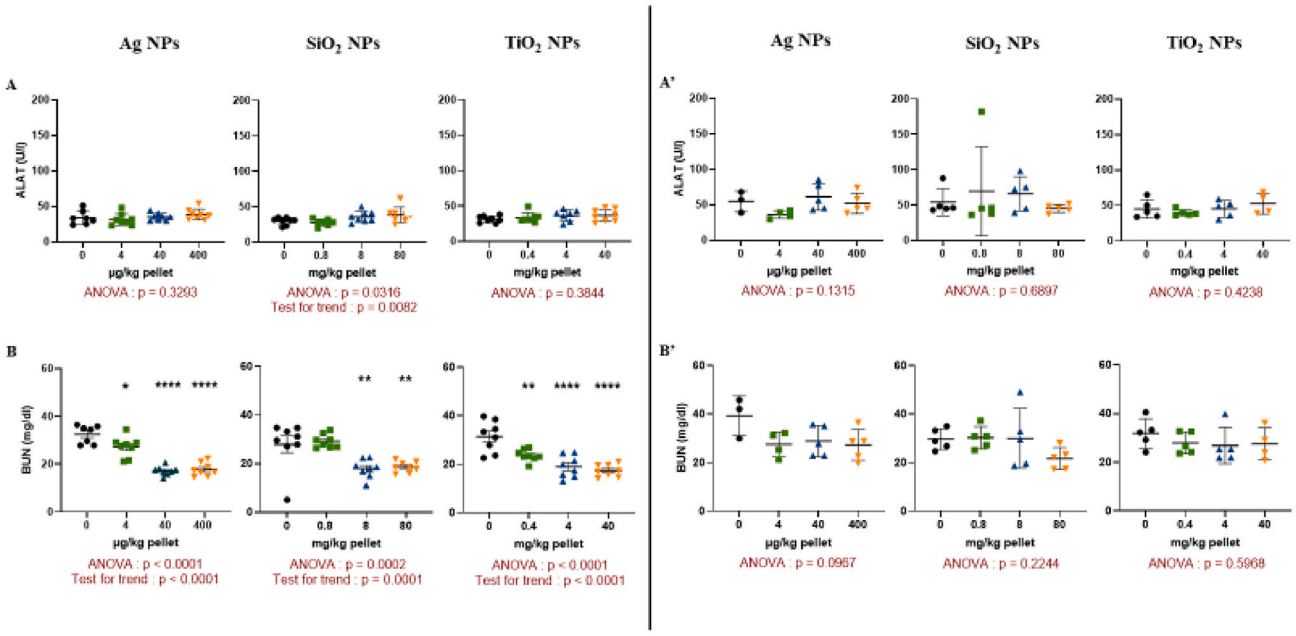


Fig. 2. Plasma ALAT and BUN responses after dietary NP exposure.
Alanine aminotransferase (A, A′) and blood urea nitrogen (B, B′) concentration after 24 weeks exposure to dietary NPs (A-B) and after 8 weeks of recovery (A′-B′). Bars represent means ± S.D. and differences between groups were analyzed by an ANOVA followed by a post-hoc Dunnett's test. *$p < 0.05$, **$p < 0.01$, ***$p < 0.001$, ****$p < 0.0001$ vs. control. The trend analysis included controls.

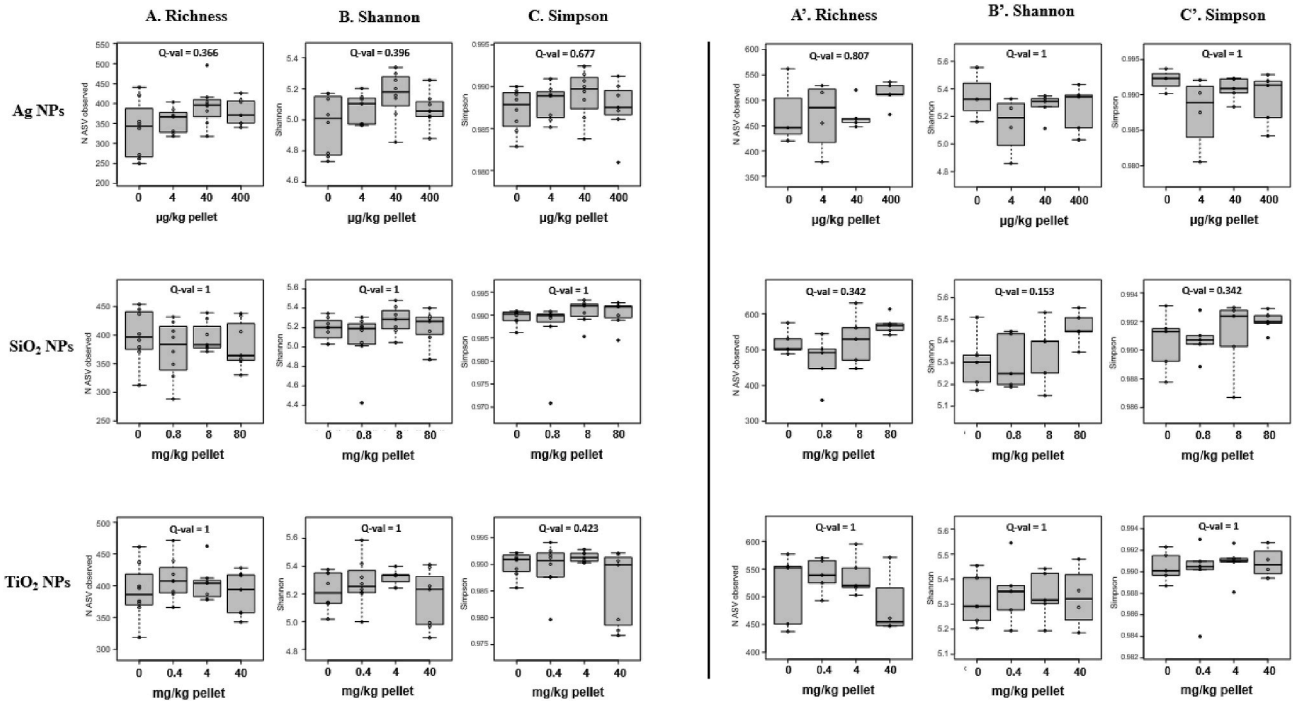


Fig. 3. Dietary exposure to NPs did not influence the α-diversity of the gut microbiota.
Mice were orally exposed to NPs during 24 weeks and α-diversity of their gut microbiota is presented as richness (number of ASV observed, A), Shannon (B) and Simpson index (C). The same analyses were conducted after a recovery period (Richness: A'; Shannon index: B'; Simpson index: C'). Individual values are represented by the circles. The bar plots represent 25th and 75th percentile with the median in the middle, whiskers depict extreme values (excluding outliers). Statistical differences among the groups were analyzed by ANOVA and a linear trend test. Q-values indicate the statistical significance of the trend test. n = 8 or 5 for end of 24 weeks of exposure and recovery, respectively.

previously observed in B6 mice after exposure to similar doses of Ag NPs (van den Brule et al., 2016).

To avoid a confounding cage effect (Laukens et al., 2016), we applied a conservative approach to analyze the β-diversity by computing the weighted UniFrac distance matrices on average bacterial profiles per cage (n = 4/5 mice per cage, N = 3 cages per dose). We found a significant dose-effect after 24 weeks exposure to Ag, SiO_2 and TiO_2 NPs, reflecting a modification of the GM profile (Fig. 4A). After the recovery

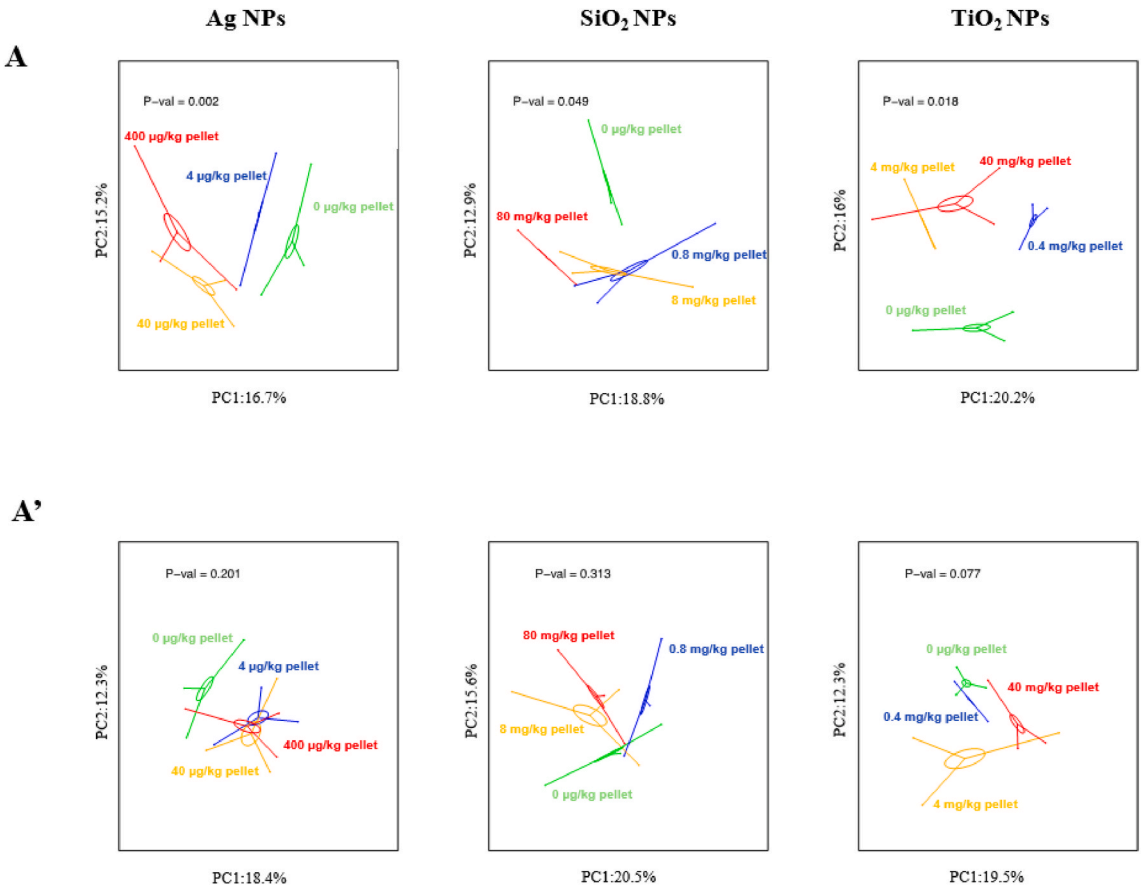


Fig. 4. Dietary NP exposure altered the β-diversity of the gut microbiota.
Principal Coordinates Analysis (PCoA) is based on weighted UniFrac distance matrices generated from all samples at the cage level at different doses. Control samples form a cluster separated from each experimental group, highlighting the proximity and the similarity of their microbial composition. After 24 weeks of exposure to dietary NPs (A). After the recovery period (8 weeks) (A'), the treatment had no significant effect. The statistical significance was assessed by ADONIS and linear trend test. *p*-values are for linear trend test.

period, no significant effect was observed (Fig. 4A'), strengthening the causal relationship between NP exposure and altered GM profile.

The relative abundance of phyla, families and genera after 24 weeks of exposure are presented as barplots in Figs. S5A–F. Analysis with linear mixed effect models built on the relative abundance mostly resulted in no significant effect of NP exposure. After Ag NPs exposure, a linear dose-dependent reduction of the relative abundance of the *Bilophila* genus was observed. *Bilophila* belongs to the Proteobacteria phylum and is generally of low abundance in the human GM. *Bilophila wadsworthia*, a Gram-negative sulfite-reducing bacteria is reportedly associated with intestinal bowel disease (Haro et al., 2016). Combined with a high fat diet, this species promotes intestinal barrier dysfunction as well as bile acid metabolism dysregulations leading to hepatic steatosis (Natividad et al., 2018). Regarding SiO_2 NPs, no significant dose-effect relationship was detected at the phylum, family or genus levels. The most significant alterations of GM structure were observed after TiO_2 NPs exposure. A dose-dependent increase of the relative abundance of Cyanobacteria, and a decrease of the Tenericutes phyla were observed. The toxicological significance of these changes is not known. Cyanobacteria are mainly studied in the marine environment, especially for their ability to produce secondary metabolites with antimicrobial or anti-proliferative activities, useful for some biotechnological applications (Mazard et al., 2016). We also observed a decrease in the relative abundance of the *Turicibacter* genera after exposure to TiO_2 NPs. A decrease in *Turicibacter* has already been observed after the ingestion of high doses of TiO_2 NPs (100 mg/kg bw/d) (Li et al., 2018), and seems to be associated with intestinal bowel disease in humans (Takahashi et al., 2016). After the recovery period, no significant impact of TiO_2 NP exposure on phyla, families and genera abundance remained (Fig. S6A'-C'), strengthening the causality of the relationship between TiO_2 NPs exposure and structural GM changes. While modifications of the GM profile have already been observed in mice 7 days after the administration of SiO_2 NPs (Chen et al., 2017) and in a dose-dependent manner after 28 days Ag NPs exposure (van den Brule et al., 2016), the impacted bacteria differ among studies. For example, we did not observe modifications of the two main phyla of the GM, Firmicutes and Bacteroidetes, associated with CM effects, and previously reported to be modified after oral administration of Ag NPs (van den Brule et al., 2016; Williams et al., 2015). The study by van den Brule et al. (2016), which used the same experimental conditions than this study (Ag NPs, doses, route of exposure) except a shorter duration of exposure (28 days), observed other changes of the GM composition than in the present study. These differences could reflect random variation, a difference in the initial composition of the GM, or an adaptation or resilience of the GM after long-term ingestion of Ag NPs. This apparent lack of consistency among studies suggests that the bacterial composition might not be an informative outcome when assessing the possible impact of NPs (or other xenobiotics) on the GM, even more so when we consider the known redundancy in GM function (Moya and Ferrer, 2016). Assessing the functional activity of the GM might, therefore, be more important, e.g. by focusing on bacterial products, such as SCFAs, known to mediate the host health responses.

3.3. Dietary NP exposure disturbed the bacterial production of SCFAs

SCFAs were quantified in cecal content after NP exposure (24 weeks) and after the recovery period (8 weeks). Acetic acid was dose-dependently reduced after exposure to SiO_2 NPs, as were propionic and butyric acids after SiO_2 (NOEL 0.2 mg/kg bw/d) and TiO_2 NPs exposure (NOEL 1 mg/kg bw/d) (Fig. 5A–C). SCFA were not affected by Ag NPs. SCFAs levels were almost restored after the recovery period in all the groups (Fig. 5A'-C'). SCFAs are produced by the GM from dietary fibers and play important roles in health and gut barrier/microbial function (Chambers et al., 2018). Altered bacterial production of SCFAs, especially butyrate, is also strongly associated with atheromatosis, diabetes and obesity (Bridgeman et al., 2020).

3.4. Systemic inflammation and circulating lipids

To further document the possible impact of NPs ingestion on the GM-CM axis, we first assessed proximal parameters known to control CM health and disease. Systemic inflammation, which contributes to the pathogenesis of atherosclerosis (Packard and Libby, 2008), was assessed by measuring the hepatic mRNA expression of two acute phase proteins, SAA-1 and IL-6 (Mieke De Buck et al., 2016). SAA-1 transcript levels were not modified by NP exposure (Fig. S7). After 24 weeks, IL-6 transcripts were not increased, but instead reduced in a dose-dependent manner after Ag and TiO_2 NP exposure (Fig. 6A). After the recovery period, IL-6 expression levels were restored in the groups exposed to Ag and TiO_2 NPs, and a significant dose-dependent reduction was observed in the group which had been fed SiO_2 NPs (Fig. 6B).

These results are in contrast with studies using higher oral doses of dietary NPs, whereby an increase in pro-inflammatory cytokines was recorded in blood after Ag NPs (Talamini et al., 2019), in the intestine after Ag (Chen et al., 2017) or TiO_2 NPs (Bettini et al., 2017), or in liver tissue after SiO_2 NPs (Ebabe Elle et al., 2013). The biological significance of the reduction of hepatic IL-6 expression recorded here remains to be clarified.

We next examined circulating lipid levels. Plasma triglyceride levels (TG) were dose-dependently reduced after 24 weeks of exposure to all NPs (Fig. 7A). Total cholesterol levels remained unaffected after exposure (Fig. 7B), and HDL-c levels were dose-dependently increased (Fig. 7C) upon Ag NPs ingestion. After the recovery period, plasma TG levels were partially restored (Fig. 7A'), whereas HDL-c levels were restored in all groups (Fig. 7C'). A decrease in blood TG has already been observed in rats after chronic ingestion of Ag NPs (500 mg/kg bw/day) or TiO_2 NPs (10 mg/kg bw/day) (Ebabe Elle et al., 2013; Chen et al., 2015). Decreased blood TG levels after Ag NPs exposure (Ebabe Elle et al., 2013) was accompanied by an increase in blood ALAT, suggesting that the liver damage caused by Ag NPs resulted in a lower hepatic production of TG. Here, we only observed a slight impact on blood ALAT after the ingestion of SiO_2 NPs, not Ag NPs (Fig. 2A), which is not consistent with an effect on TG resulting from hepatic toxicity. A first hypothesis might involve IL-6. In a murine model of non-alcoholic fatty liver disease, treatment with microRNA-26a induced a reduction of hepatic IL-6 expression which went paired with decreased TG liver levels (He et al., 2017). As we observed a lower hepatic IL-6 expression after exposure to all NPs (Fig. 6), this could be associated with a reduced production of TG in the liver, resulting in decreased blood TG levels. Second, as SCFAs can inhibit intracellular lipolysis and increase the extraction of triglycerides, regulating lipid metabolism (He et al., 2020; Canfora et al., 2015), the reductions in cecal SCFAs content recorded in the present study may also contribute to explain the reduction in blood TG observed after 24 weeks of treatment. A third possibility is an impaired lipid digestion or absorption directly induced by the presence of the NPs in the gastrointestinal tract, resulting in reduced blood TG levels, as already reported with cellulose nanomaterials (DeLoid et al., 2018), but not with TiO_2 NPs (Li et al., 2017b).

The TG/HDL-c ratio, an index of atherogenic risk (da Luz et al.,

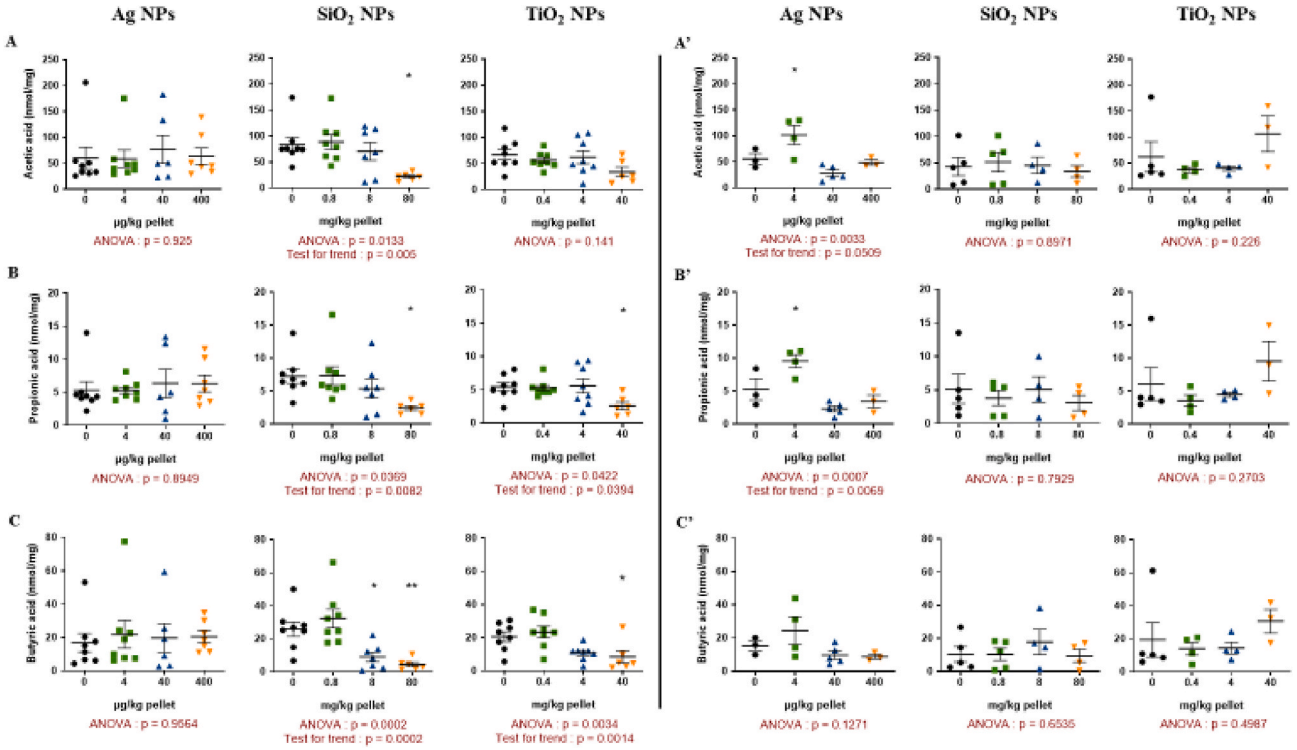


Fig. 5. Cecal levels of the main short chain fatty acids (SCFAs) were disturbed after 24 weeks of exposure to dietary NP.
Acetic acid (**A, A'**), propionic acid (**B,B'**) and butyric acid (**C,C'**) were measured in the cecal content after 24 weeks exposure to dietary NP (A-C) and after 8 weeks of recovery (A'-C'). Bars represent means ± S.D. and differences between groups were analyzed by an ANOVA followed by a post-hoc Dunnett's test. $*p < 0.05$, $**p < 0.01$ vs. control. The trend analysis included controls.

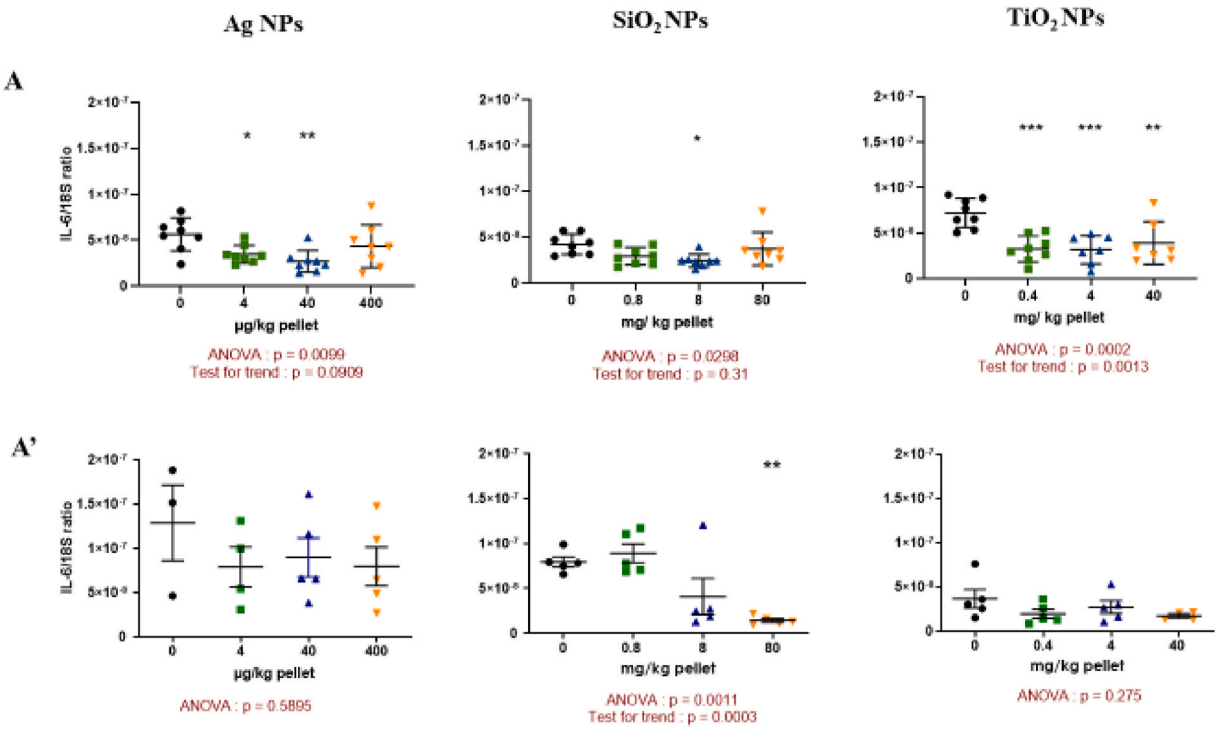


Fig. 6. Hepatic IL-6 expression after dietary NP exposure.
The expression of IL-6 was quantified by RT-qPCR in the liver (A: after the exposure, 24 weeks; A': after the recovery period, 8 weeks). Gene expression was normalized to 18S rRNA amplified on the same sample. Bars represent means ± S.D. and differences between groups were analyzed by an ANOVA followed by a post-hoc Dunnett's test. *p < 0.05, **p < 0.01, ***p < 0.001 vs. control. The trend analysis included controls.

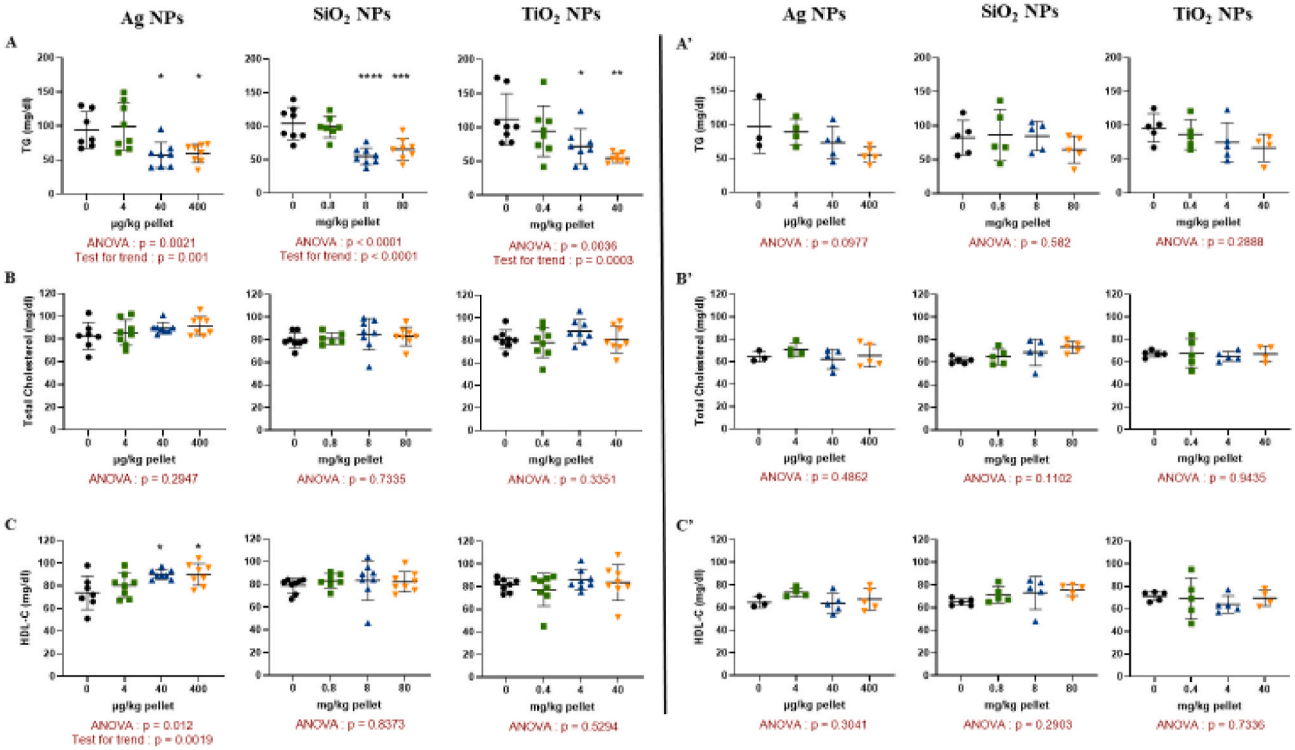


Fig. 7. Dietary NP exposure reduced circulating TG levels.
Plasma triglyceride (A, A′), total cholesterol (B, B′) and HDL-cholesterol (C, C′) concentration after 24 weeks exposure to dietary NP (A-C) and after 8 weeks of recovery (A′-C′). Bars represent means ± S.D. and differences between groups were analyzed by an ANOVA followed by a post-hoc Dunnett's test. *$p < 0.05$, **$p < 0.01$, ***$p < 0.001$, ****$p < 0.0001$ vs. control. The trend analysis included controls.

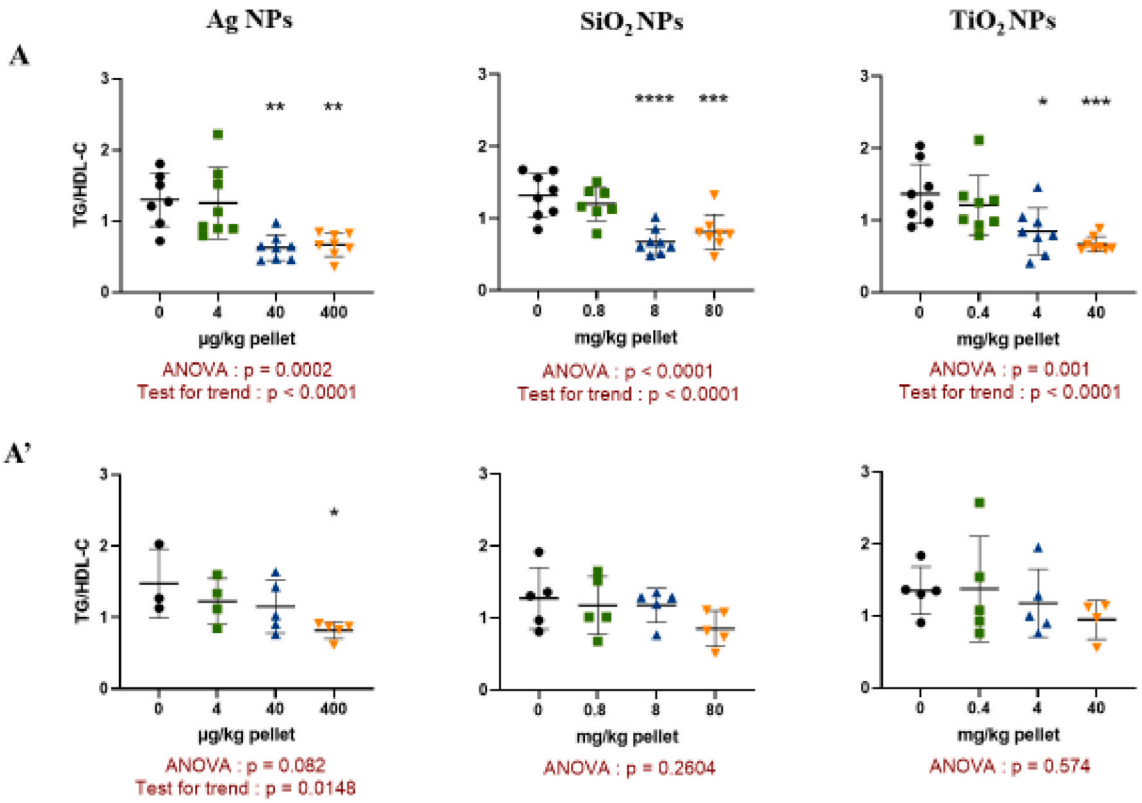


Fig. 8. Dietary NP exposure reduced the TG/HDL-c ratio.
Triglycerides/HDL-cholesterol ratio (A, A′) after 24 weeks exposure to dietary NP (A) and after 8 weeks of recovery (A′). Bars represent means ± S.D. and differences between groups were analyzed by an ANOVA followed by a post-hoc Dunnett's test. *$p < 0.05$, **$p < 0.01$, ***$p < 0.001$, ****$p < 0.0001$ vs. control. The trend analysis included controls.

2008), was dose-dependently decreased for all NPs (Fig. 8A). After the recovery period, the TG/HDL-c ratio was only partially restored (Fig. 8A').

3.5. No CM toxicity was recorded after dietary NP exposure

Finally, we assessed two distal CM endpoints, glucose homeostasis and atheromatosis, after dietary exposure.

Twenty weeks after oral exposure to Ag, SiO_2 or TiO_2 NPs, blood glucose homeostasis was not affected (Fig. S8). This observation is in contrast with the results of Chen et al. (2020) who reported impaired blood glucose homeostasis in rats exposed to TiO_2 NPs (0, 2, 10 and 50 mg/kg/d) in combination with glucose (1.8 g/kg/d) for 90 days.

After 24 weeks of NP exposure, we stained thoracic aortas with Oil Red O to reveal lipid deposits indicative of atheromatous plaque formation. No excessive fat deposition was observed neither in controls mice or mice exposed to NPs (Fig. 9).

These results are also in contrast to earlier studies reporting that NPs tend to favor the development of cardiovascular outcomes. Oral ingestion of 10 mg TiO_2 NPs/kg bw/d resulted in a decrease in heart rate and systolic blood pressure and an increase in diastolic blood pressure in rats (Chen et al., 2015). Impaired vasomotor function was also observed after 10 weeks exposure to TiO_2 NPs at similar doses in vivo and ex vivo on rat aorta rings, and ex vivo on subcutaneous human arteries (Jensen et al., 2018a, 2018b). Moreover, particles such as ambient ultrafine particles are known to promote cardiovascular diseases (Robertson and Miller, 2018; Rajagopalan et al., 2018). In contrast, oral administration of diesel exhaust particles appeared to reduce plaque areas on thoracic aortas in ApoE-deficient mice (van den Brule et al., 2021), suggesting a protective action of NPs on atheromatous outcomes. Our results (reduced hepatic IL-6 expression, decreased circulating TG levels and TG/HDL-c ratios) would be consistent with such a protective effect of dietary NPs.

4. Conclusion

We found that long-term oral exposure to dietary NPs in mice, at doses relevant for estimated human intakes, did not cause overt toxicity, but dose-dependently and reversibly disrupted the composition (Ag, TiO_2 and SiO_2 NPs) of the GM and the production of bacterial SCFA (TiO_2 and SiO_2 NPs). These GM alterations were not associated with an atheromatous disease or with altered glucose homeostasis. Instead, some apparently beneficial responses, including a reduction of the pro-inflammatory master cytokine IL-6 and of circulating TG levels, were recorded after NP exposure (Ag, TiO_2 and SiO_2 NPs). It remains to understand how the latter effects are induced by NPs and whether GM changes are involved.

Submission declaration

This manuscript has not been published previously, is not under consideration for publication elsewhere and its publication is approved by all authors and tacitly or explicitly by the responsible authorities, where the work was carried out. If accepted, this manuscript will not be published elsewhere in the same form, in English or in any other language, including electronically without the written consent of the copyright-holder.

Ethics declaration

All animal experiments were approved by the local committee for animal research at the Université catholique de Louvain, Comité

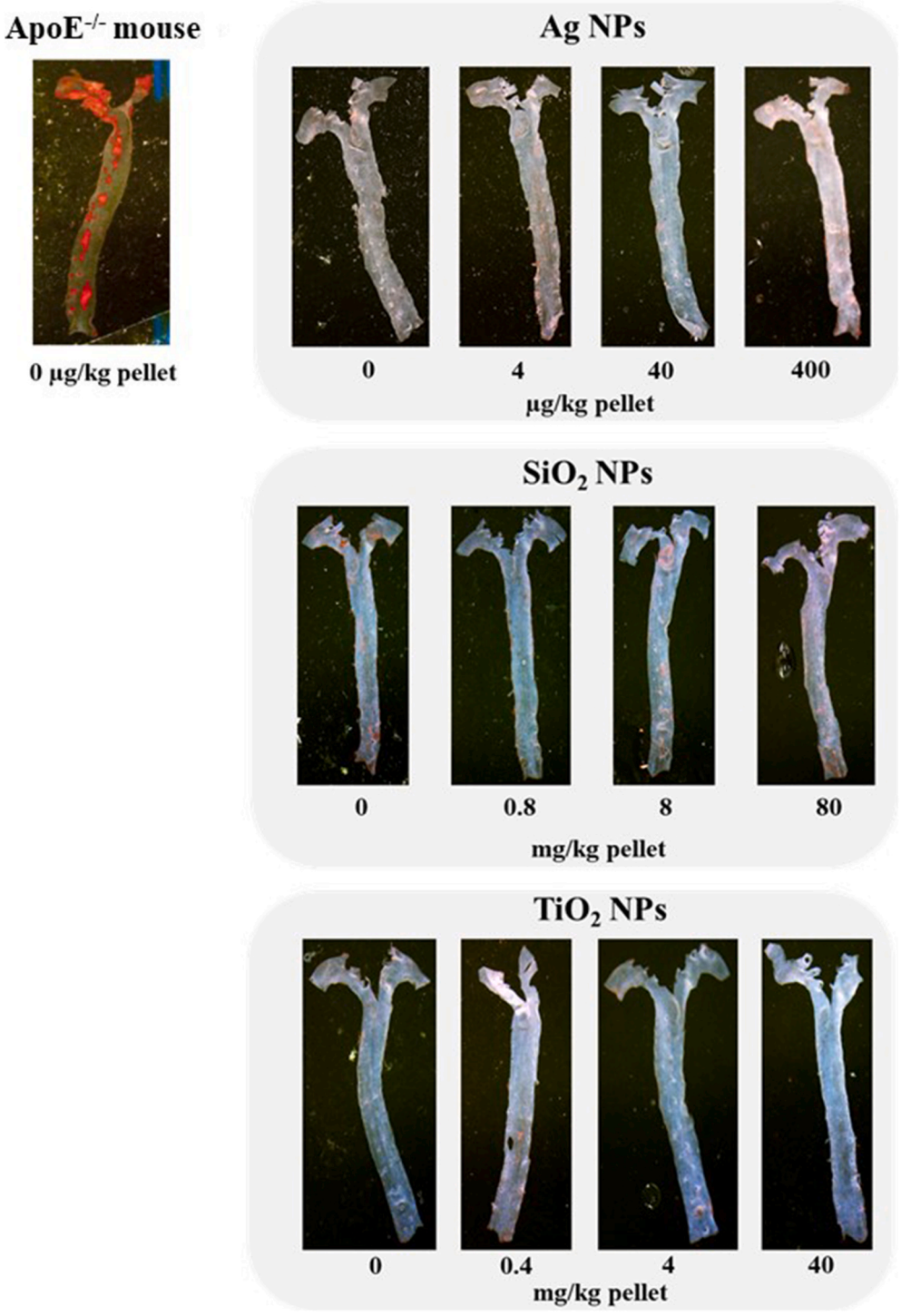


Fig. 9. Dietary NP exposure did not promote atheromatous plaque formation in B6 male mice.
The presence of fatty deposits in thoracic aortas was assessed in 4 mice per group using Oil Red O staining, and was examined *en face* under a binocular microscope (16X magnification). Representative images are shown. An example of atheromatous aorta in an ApoE-deficient mouse is shown as a positive control (upper left corner).

d'Ethique pour l'Expérimentation Animale, Secteur des Sciences de la Santé, Brussels, Belgium (No LA1230312).

Funding

This study was supported by a grant from the Fonds de la Recherche Scientifique (FRS-FNRS) under grant N° PDR T.0151.19.

CRediT authorship contribution statement

Laeticia Perez: conceived, designed and supervised the experimental work, and drafted the manuscript. **Eleonora Scarcello:** conceived, designed and supervised the experimental work, and drafted the manuscript. **Saloua Ibouraadaten:** executed the experiments, acquired, analyzed and interpreted the data. **Yousof Yakoub:** executed the experiments, acquired, analyzed and interpreted the data. **Riccardo Leinardi:** executed the experiments, acquired, analyzed and interpreted the data. **Jérôme Ambroise:** analyzed and interpreted the metagenomics data. **Bertrand Bearzatto:** analyzed and interpreted the metagenomics data. **Jean-Luc Gala:** analyzed and interpreted the metagenomics data. **Adrien Paquot:** contributed to the SCFA analysis. **Giulio G. Muccioli:** contributed to the SCFA analysis. **Caroline Bouzin:**

contributed to the atheroma analyses and their interpretation. **Sybille van den Brule:** conceived, designed and supervised the work, and wrote the manuscript. **Dominique Lison:** conceived, designed and supervised the work, and wrote the manuscript, All authors read and approved the final manuscript.

Declaration of competing interest

The authors declare that they have no known competing financial interests or personal relationships that could have appeared to influence the work reported in this paper.

Appendix A. Supplementary data

Supplementary data to this article can be found online at https://doi.org/10.1016/j.fct.2021.112352.

References

Bettini, S., et al., 2017. Food-grade TiO2 impairs intestinal and systemic immune homeostasis, initiates preneoplastic lesions and promotes aberrant crypt development in the rat colon. Sci. Rep. 7, 40373.

Bokulich, N.A., et al., 2013. Quality-filtering vastly improves diversity estimates from Illumina amplicon sequencing. Nat. Methods 10 (1), 57–59.

Bowe, J.E., et al., 2014. Metabolic phenotyping guidelines: assessing glucose homeostasis in rodent models. J. Endocrinol. 222 (3), G13–G25.

Bridgeman, S.C., et al., 2020. Butyrate generated by gut microbiota and its therapeutic role in metabolic syndrome. Pharmacol. Res. 160, 105174.

Callahan, B.J., et al., 2016. DADA2: high-resolution sample inference from Illumina amplicon data. Nat. Methods 13 (7), 581–583.

Canfora, E.E., Jocken, J.W., Blaak, E.E., 2015. Short-chain fatty acids in control of body weight and insulin sensitivity. Nat. Rev. Endocrinol. 11 (10), 577–591.

Chambers, E.S., et al., 2018. Role of gut microbiota-generated short-chain fatty acids in metabolic and cardiovascular health. Curr. Nutr. Rep. 7 (4), 198–206.

Chassaing, B., et al., 2012. Fecal lipocalin 2, a sensitive and broadly dynamic non-invasive biomarker for intestinal inflammation. PLoS One 7 (9), e44328.

Chaudhry, Q., et al., 2008. Applications and implications of nanotechnologies for the food sector. Food Addit. Contam. Part A Chem Anal Control Expo Risk Assess 25 (3), 241–258.

Chen, Z., et al., 2015. Effect of titanium dioxide nanoparticles on the cardiovascular system after oral administration. Toxicol. Lett. 239 (2), 123–130.

Chen, H., et al., 2017. The effects of orally administered Ag, TiO 2 and SiO 2 nanoparticles on gut microbiota composition and colitis induction in mice. NanoImpact 8, 80–88.

Chen, Z., et al., 2019a. Hepatotoxicity and the role of the gut-liver axis in rats after oral administration of titanium dioxide nanoparticles. Part. Fibre Toxicol. 16 (1), 48.

Chen, Z., et al., 2019b. Effects of oral exposure to titanium dioxide nanoparticles on gut microbiota and gut-associated metabolism in vivo. Nanoscale 11 (46), 22398–22412.

Chen, Z., et al., 2020. Combined effect of titanium dioxide nanoparticles and glucose on the blood glucose homeostasis in young rats after oral administration. J. Appl. Toxicol. 40 (9), 1284–1296.

Collins, C.M., D'Orazio, S.E., 1993. Bacterial ureases: structure, regulation of expression and role in pathogenesis. Mol. Microbiol. 9 (5), 907–913.

da Luz, P.L., et al., 2008. High ratio of triglycerides to HDL-cholesterol predicts extensive coronary disease. Clinics 63 (4), 427–432.

Dekkers, S., et al., 2011. Presence and risks of nanosilica in food products. Nanotoxicology 5 (3), 393–405.

DeLoid, G.M., et al., 2018. Reducing intestinal digestion and absorption of fat using a nature-derived biopolymer: interference of triglyceride hydrolysis by nanocellulose. ACS Nano 12 (7), 6469–6479.

Dorier, M., et al., 2017. Continuous in vitro exposure of intestinal epithelial cells to E171 food additive causes oxidative stress, inducing oxidation of DNA bases but no endoplasmic reticulum stress. Nanotoxicology 11 (6), 751–761.

Ebabe Elle, R., et al., 2013. Dietary exposure to silver nanoparticles in Sprague-Dawley rats: effects on oxidative stress and inflammation. Food Chem. Toxicol. 60, 297–301.

Fiordaliso, F., et al., 2018. Realistic evaluation of titanium dioxide nanoparticle exposure in chewing gum. J. Agric. Food Chem. 66 (26), 6860–6868.

Fruijtier-Polloth, C., 2016. The safety of nanostructured synthetic amorphous silica (SAS) as a food additive (E 551). Arch. Toxicol. 90 (12), 2885–2916.

Hadrup, N., et al., 2012. Subacute oral toxicity investigation of nanoparticulate and ionic silver in rats. Arch. Toxicol. 86 (4), 543–551.

Hajipour, M.J., et al., 2012. Antibacterial properties of nanoparticles. Trends Biotechnol. 30 (10), 499–511.

Haro, C., et al., 2016. Intestinal microbiota is influenced by gender and body mass index. PLoS One 11 (5), e0154090.

He, Q., et al., 2017. MicroRNA-26a-interleukin (IL)-6-IL-17 axis regulates the development of non-alcoholic fatty liver disease in a murine model. Clin. Exp. Immunol. 187 (1), 174–184.

He, J., et al., 2020. Short-chain fatty acids and their association with signalling pathways in inflammation, glucose and lipid metabolism. Int. J. Mol. Sci. 21 (17).

Hill, M.J., Drasar, B.S., 1975. The normal colonic bacterial flora. Gut 16 (4), 318–323.

Hochberg, Y.B.a.Y., 1995. Controlling the false discovery rate: a practical and powerful approach to multiple testing. J. Roy. Stat. Soc. B 57 (1), 289–300.

Hornung, B.V.H., Zwittink, R.D., Kuijper, E.J., 2019. Issues and current standards of controls in microbiome research. FEMS Microbiol. Ecol. 95 (5).

Hugenholtz, F., de Vos, W.M., 2018. Mouse models for human intestinal microbiota research: a critical evaluation. Cell. Mol. Life Sci. 75 (1), 149–160.

Jensen, D.M., et al., 2018a. Vasomotor function in rat arteries after ex vivo and intragastric exposure to food-grade titanium dioxide and vegetable carbon particles. Part. Fibre Toxicol. 15 (1), 12.

Jensen, D.M., et al., 2018b. Vasomotor dysfunction in human subcutaneous arteries exposed ex vivo to food-grade titanium dioxide. Food Chem. Toxicol. 120, 321–327.

Kennedy, A.J., et al., 2010. Mouse models of the metabolic syndrome. Dis. Models Mechan. 3 (3–4), 156–166.

Kim, J.H., et al., 2014. Immunotoxicity of silicon dioxide nanoparticles with different sizes and electrostatic charge. Int. J. Nanomed. 9 (Suppl. 2), 183–193.

Klindworth, A., et al., 2013. Evaluation of general 16S ribosomal RNA gene PCR primers for classical and next-generation sequencing-based diversity studies. Nucleic Acids Res. 41 (1), e1.

Kong, G., et al., 2020. Microbiome profiling reveals gut dysbiosis in a transgenic mouse model of Huntington's disease. Neurobiol. Dis. 135, 104268.

Laukens, D., et al., 2016. Heterogeneity of the gut microbiome in mice: guidelines for optimizing experimental design. FEMS Microbiol. Rev. 40 (1), 117–132.

Li, R., et al., 2017a. Ambient ultrafine particle ingestion alters gut microbiota in association with increased atherogenic lipid metabolites. Sci. Rep. 7, 42906.

Li, Q., et al., 2017b. Potential impact of inorganic nanoparticles on macronutrient digestion: titanium dioxide nanoparticles slightly reduce lipid digestion under simulated gastrointestinal conditions. Nanotoxicology 11 (9–10), 1087–1101.

Li, J., et al., 2018. Oral administration of rutile and anatase TiO2 nanoparticles shifts mouse gut microbiota structure. Nanoscale 10 (16), 7736–7745.

Mazard, S., et al., 2016. Tiny microbes with a big impact: the role of Cyanobacteria and their metabolites in shaping our future. Mar. Drugs 14 (5).

McClements, D.J., Xiao, H., 2017. Is nano safe in foods? Establishing the factors impacting the gastrointestinal fate and toxicity of organic and inorganic food-grade nanoparticles. NPJ Sci. Food 1, 6.

Meike van der Zande, R.J.V., J Groot, Maria, Kramer, Evelien, Herrera Rivera, Zahira E., Rasmussen, Kirsten, Ossenkoppele, Jan S., Tromp, Peter, Gremmer, Eric R., Peters, Ruud JB., Hendriksen, Peter J., Marvin, Hans JP., LAP Hoogenboom, Ron, 2014. Ad ACM Peijnenburg and Hans Bouwmeester, *Sub-chronic toxicity study in rats orally exposed to nanostructured silica.* Part. Fibre Toxicol. 11 (8).

Mieke De Buck, M.G., Wang, Ji Ming, Van Snickc, Jacques, Opdenakker, Ghislain, Struyf, Sofie, Jo Van Damme, 2016. Structure and expression of different serum amyloid A (SAA) variants and their concentration-dependent functions during host insults. Curr. Med. Chem. 23, 1725–1755.

Morselli, E., et al., 2017. The effects of oestrogens and their receptors on cardiometabolic health. Nat. Rev. Endocrinol. 13 (6), 352–364.

Moya, A., Ferrer, M., 2016. Functional redundancy-induced stability of gut microbiota subjected to disturbance. Trends Microbiol. 24 (5), 402–413.

Mu, W., et al., 2019. Effect of long-term intake of dietary titanium dioxide nanoparticles on intestine inflammation in mice. J. Agric. Food Chem. 67 (33), 9382–9389.

Murugadoss, S., et al., 2017. Toxicology of silica nanoparticles: an update. Arch. Toxicol. 91 (9), 2967–3010.

Mutlu, E.A., et al., 2018. Inhalational exposure to particulate matter air pollution alters the composition of the gut microbiome. Environ. Pollut. 240, 817–830.

Natividad, J.M., et al., 2018. Bilophila wadsworthia aggravates high fat diet induced metabolic dysfunctions in mice. Nat. Commun. 9 (1), 2802.

O'Hara, A.M., Shanahan, F., 2006. The gut flora as a forgotten organ. EMBO Rep. 7 (7), 688–693.

Orr, S.E., et al., 2019. Alteration in the mRNA expression of genes associated with gastrointestinal permeability and ileal TNF-alpha secretion due to the exposure of silver nanoparticles in Sprague-Dawley rats. J. Nanobiotechnol. 17 (1), 63.

Packard, R.R., Libby, P., 2008. Inflammation in atherosclerosis: from vascular biology to biomarker discovery and risk prediction. Clin. Chem. 54 (1), 24–38.

Pascale, A., et al., 2018. Microbiota and metabolic diseases. Endocrine 61 (3), 357–371.

Pietroiusti, A., et al., 2017. The unrecognized occupational relevance of the interaction between engineered nanomaterials and the gastro-intestinal tract: a consensus paper from a multidisciplinary working group. Part. Fibre Toxicol. 14 (1), 47.

Rajagopalan, S., Al-Kindi, S.G., Brook, R.D., 2018. Air pollution and cardiovascular disease: JACC state-of-the-art review. J. Am. Coll. Cardiol. 72 (17), 2054–2070.

Rasmussen K, M.A, Mast J, De Temmerman P, Waegeneers N, Van Steen F, Pizzolon J, De Temmerman L, Van Doren E, Jensen K, Birkedal R, Levin M, Nielsen S, Koponen I, Clausen P, Kembouche Y, Thieriet N, Spalla O, Giuot C, Rousset D, Witschger O, Bau S, Bianchi B, Shivachev B, Gilliland D, Pianella F, Ceccone G, Cotogno G, Rauscher H, Gibson P, Stamm H. , Synthetic Amorphous Silicon Dioxide (NM-200, NM-201, NM-202, NM-203, NM-204): Characterisation and Physico-Chemical Properties. 2013: Luxembourg (Luxembourg): .

Rasmussen K, M.J, De Temmerman P, Verleysen E, Waegeneers N, Van Steen F, Pizzolon J, De Temmerman L, Van Doren E, Jensen K, Birkedal R, Levin M, Nielsen S, Koponen I, Clausen P, Kofoed-Sørensen V, Kembouche Y, Thieriet N, Spalla O, Giuot C, Rousset D, Witschger O, Bau S, Bianchi B, Motzkus C, Shivachev B, Dimowa L, Nikolova R, Nihtianova D, Tarassov M, Petrov O, Bakardjieva S, Gilliland D, Pianella F, Ceccone G, Spampinato V, Cotogno G, Gibson P, Gaillard C, Mech A, Titanium Dioxide, NM-100, NM-101, NM-102, NM-103, NM-104, NM-105: Characterisation and Physico-Chemical Properties. 2014: Luxembourg (Luxembourg).

Robertson, S., Miller, M.R., 2018. Ambient air pollution and thrombosis. Part. Fibre Toxicol. 15 (1), 1.
Russell, J.C., Proctor, S.D., 2006. Small animal models of cardiovascular disease: tools for the study of the roles of metabolic syndrome, dyslipidemia, and atherosclerosis. Cardiovasc. Pathol. 15 (6), 318–330.
So, S., Jang, I.-S., Han, C., 2008. Effect of micro/nano silica particle feeding for mice. J. Nanosci. Nanotechnol. 8, 5367–5371.
Takahashi, K., et al., 2016. Reduced abundance of butyrate-producing bacteria species in the fecal microbial community in crohn's disease. Digestion 93 (1), 59–65.
Talamini, L., et al., 2019. Repeated administration of the food additive E171 to mice results in accumulation in intestine and liver and promotes an inflammatory status. Nanotoxicology 13 (8), 1087–1101.
van den Brule, S., et al., 2016. Dietary silver nanoparticles can disturb the gut microbiota in mice. Part. Fibre Toxicol. 13 (1), 38.
van den Brule, S., et al., 2021. Diesel exhaust particles alter the profile and function of the gut microbiota upon subchronic oral administration in mice. Part. Fibre Toxicol. 18 (1), 7.
Wang, W., et al., 2018. Exposure to concentrated ambient PM2.5 alters the composition of gut microbiota in a murine model. Part. Fibre Toxicol. 15 (1), 17.
Weir, A., et al., 2012. Titanium dioxide nanoparticles in food and personal care products. Environ. Sci. Technol. 46 (4), 2242–2250.
Wilding, L.A., et al., 2016. Repeated dose (28-day) administration of silver nanoparticles of varied size and coating does not significantly alter the indigenous murine gut microbiome. Nanotoxicology 10 (5), 513–520.
Williams, K., et al., 2015. Effects of subchronic exposure of silver nanoparticles on intestinal microbiota and gut-associated immune responses in the ileum of Sprague-Dawley rats. Nanotoxicology 9 (3), 279–289.
Yoshida, T., et al., 2014. Intestinal absorption and biological effects of orally administered amorphous silica particles. Nanoscale Res. Lett. 9 (1), 532.
Younes, M., et al., 2021. Safety assessment of titanium dioxide (E171) as a food additive. EFSA J. 19 (5), e06585.